Controllable preparation of metal nanoparticle arrays by a micellar route

JING-JING DONG*, XUE-FEN WANG, JIANG-LONG JI, HUI-YING HAO, JIE XING, ZHEN-JUN FAN
School of Science, China University of Geosciences (Beijing), 29 Xue Yuan Road, Haidian District, Beijing, 100083, China

Ordered arrays of metal nanoparticles were prepared by a micellar route based on the self-assembly of a diblock copolymer to micelles. Taking advantage of this route, the size and interparticle spacing of the metal nanoparticle arrays were tuned effectively by varying the chain length of the ramphiphilic diblock copolymer, the amount of metal salt loading, and the drawing velocity during dip-coating process. As an application example of Au nanoparticle arrays, the characteristics of localized surface plasmon (LSP) were studied by varying the interparticle spacing.

(Received April 17, 2014; accepted May 15, 2014)

Keywords: Nanoparticle, Reverse micelle, copolymer, Localized surface plasmon

1. Introduction

Metal nanoparticles (Au, Ag, Pt et al.) are of great interest for various scientific and technical applications because of their unique optical [1, 2], magnetic [3, 4], and catalytic [5, 6] properties compared with bulk materials. This is even more the case if the particle size and interparticle spacing can be controlled flexibly. For example, the size-dependent interaction of light with metal nanoparticles, which is referred to as localized surface plasmon (LSP) [7], can enhance the performance of light-emitting diodes (LEDs) and solar cells greatly [8, 9]. So far, various approaches have been tried to prepare metal nanoparticles with well-defined particle size and interparticle spacing. Among them, top-down procedures, such as electron beam lithography, X-ray lithography and so on, offer the advantage of high-precision, but they are rather complicated, time-consuming and expensive. An alternative route is the so-called bottom-up technology, which relies on the self-organization of larger molecules as building blocks for the resulting nanostructures. Well-known examples of bottom-up technology are nanosphere lithography, scanning probe microscopy and micro-contact printing techniques, however they suffer from poor flexibility, low throughput and substrate limitation respectively. Therefore, a substrate-independent, low-cost and simple technique with the flexibility to control the particle size and interparticle spacing is desirable.

The approach described here is based on the self-assembly of a diblock copolymer to micelles. The basic idea is to use spherical reverse micelles, which form when a diblock copolymer consisting of a hydrophilic and a hydrophobic block is dissolved in a polar solvent such as toluene. Then, the diblock copolymer micelles are loaded with chemical precursors such as metal salts, and deposited as a micellar mono film onto a substrate via various coating technologies. Finally, the diblock copolymer is removed by means of hydrogen or oxygen plasma, leaving behind regularly arranged and uniform metal nanoparticles. Although this micellar method has been reported earlier [2, 10], a comprehensive and detailed study of various factors on the morphology of the metal nanoparticles is essential. In this paper, the size and interparticle spacing of the metal nanoparticles are tuned by varying the chain length of the amphiphilic diblock copolymer, the amount of metal salt loaded, and the parameters during coating process effectively.

2. Experimental procedure

Taking Au nanoparticles for example, the fabrication process is schematically illustrated in Fig. 1. First, a diblock copolymer poly(styrene) -block-poly (2-vinylpyridine), i.e. PS-P2VP, is dissolved in toluene, and the solution was stirred for three days allowing the PS-P2VP to self-assemble into inverse micelles with P2VP blocks forming the cores and PS blocks forming the shells. Next, $HAuCl_4$ was added into the micellar solution with a constant total loading L (the loading is defined as $L = n(\text{salt})/n(\text{P2VP})$). Finally, the solution is stirred for more than five days allowing metal salts to be loaded into the PS-P2VP micelles completely and homogeneously. All the process is carried out at room temperature. To deposit the metal-salt-loaded micelles onto substrates, the micelles loaded with metal salts were deposited on Si substrates by a dip-coating or spin-coating process, as described in the

previous report [3], and then well-ordered hexagonal arrays of metal-salt-loaded micelles are obtained. In order to remove the polymer matrix and reduce the metal salts into their metallic states, the as-coated samples were subsequently subjected to hydrogen plasma treatment for 30 min (150 Pa, 100 W) within a home-made radio frequency plasma system.

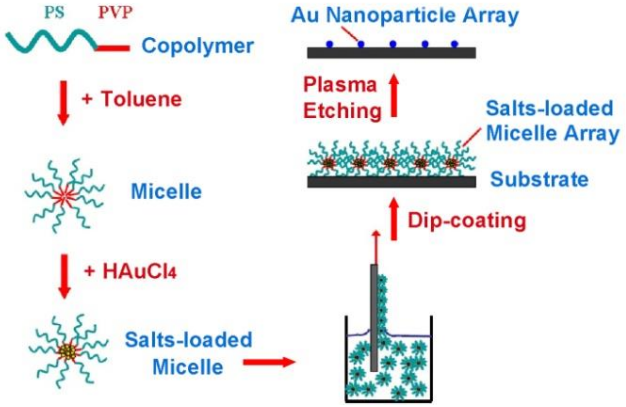

Fig. 1. (black/white) Schematic illustration of the fabrication process of the Au nanoparticles by the micellar route.

The morphologies of the micelle or metal nanoparticle arrays are characterized by atomic force microscopy (AFM) using an NT-MDT Solver P47 in a semi-contact mode. The optical transmittance and reflection spectra were measured as a function of incident photon wavelength at wavelengths between 200 and 800 nm from Au nanoparticles using a Shimadzu UV-3101 spectrophotometer. The spectrophotometer was used in a double-beam mode with a bare substrate in the reference beam to obtain transmittance data through the film alone.

3. Results and discussions

Due to the self-assembly of micelles on the Si substrate, the closely packed metal-salt-loaded micelle array was obtained by a dip-coating process, as shown in Fig. 2a. It can be seen that the micelle array presents good monodispersity and quasi hexagonal order.

As mentioned above, H plasma treatment was introduced to remove the polymer matrix and reduce the metal salt of the metal-salt-loaded micelle array. To observe the morphology evolution of the metal-salt-loaded micelles during H plasma treatment, AFM measurements were performed after exposure to H plasma for 1, 5, 15, and 30 min under 150 Pa, 50 W respectively, and the corresponding AFM images are shown in Figs. 2b-2e. Here, the micelle in use is PS(1760)-P2VP(100), and the metal salt is $HAuCl_4$. It can be seen that the size of micelle particles decreases gradually with the etching time, while the monodispersity and quasi hexagonal order are conserved well throughout the H plasma treatment, indicating that the carefully designed etching process has little influence on the order of the micelle array.

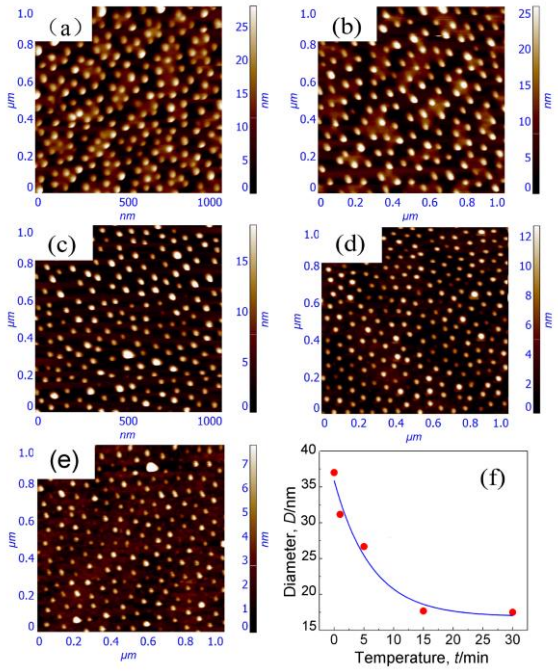

Fig. 2. (black/white) AFM topography images of $HAuCl_4$-loaded micelle array (a) before and after exposure to H plasma for (b) 1, (c) 5, (d) 15, and (e) 30 min under 150 Pa, 50 W. (f) plot of the micelle particle size as a function of the H plasma etching time.

The size of micelle particle as a function of the H plasma etching time has been plotted as shown in Fig. 2f. In agreement with the curve evolution, the results can be fitted with the law:

$$D = 19 \times e^{-(t/6.26)} + 16.13 \qquad (1)$$

where D is the diameter of the micelle particle, and t accounts for the H plasma etching time. From the plot in Fig. 2f, we can see that at the beginning of the etching, the size of the micelle particle decreases quickly as a result of the fast etching rate of the organic matrix, however the decrease become relatively slow after H plasma exposure for 15 minutes, suggesting that most of the organic matrix has been removed. Being etched for 30 minutes, the size of the micelle particle remained almost unchanged compared with the size of micelle particle etching for 15 minutes, indicating that the organic matrix has been removed completely.

One of the advantages of the micellar method is that the size and interparticle spacing of the metal nanoparticles can be tuned conveniently and effectively, whch is highly desirable for various scientific and technical applications. So, we adjusted the size and interparticle spacing of the metal nanoparticle arrays by varying the chain length of the amphiphilic diblock copolymer, the amount of metal salt loading, and the drawing velocity during dip-coating process.

First we tried to adjust the size and interparticle spacing by changing the chain length of the involved copolymer, i.e. the number of repeat units (m, n) of amphiphilic diblock copolymer PS(n)-P2VP(m) in use. The interparticle spacing is related to total chain length m+n, and longer total chain length leads to larger interparticle spacing. While the size of metal nanoparticles only depends on the chain length of kernel P2VP (m) in fixed metal salt, because a longer P2VP block contain more pyridine monomers which is able to incorporate more metal salt for each micelle, and consequently form a bigger metal nanoparticle. Figs. 3a-3d show the typical AFM images of Au nanoparticle arrays by using the copolymer PS(3620)-P2VP(100), PS(1760)-P2VP(308), PS(1760)-P2VP(700), and PS(306)-P2VP(125) respectively. Obviously, both the size and interparticle spacing vary greatly with the chain length of the copolymer in use. According to the data derived from the AFM images shown in Figs. 3a-3d, the corresponding diameters of Au nanoparticles by using the copolymer PS(3620)-P2VP(100), PS(1760)-P2VP(308), PS(1760)-P2VP(700) and PS(306)-P2VP(125) are 18, 30, 45 and 20 nm, and the center-to-center (CTC) distances of the neighboring Au nanoparticles are 140, 90, 100 and 45 nm respectively, which is in accord with the analysis mentioned earlier.

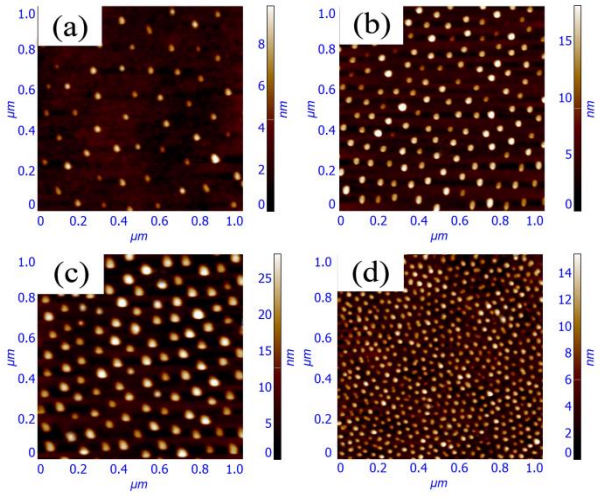

Fig. 3. (black/white) AFM topography images of Au nanoparticle arrays by using the copolymer (a) PS(3620) - P2VP (100), (b) PS (1760) - P2VP (308), (c) PS(1760)-P2VP(700), (d) PS(306)-P2VP(125).

Although the size and interparticle spacing of metal nanoparticles can be tuned by varying the chain length of the copolymer in use, the range is limited by the copolymer commercially available. So then we tried to adjust the particle size and interparticle spacing by varying the amount of metal salt loading and the drawing velocity during the dip-coating process in the following.

As mentioned above, a longer P2VP block contain more pyridine monomers which is able to incorporate more metal salt for each micelle, and consequently form a bigger metal nanoparticle. So, fixing the PS-P2VP block copolymers in use, the number of pyridine monomer contained in each micelle is definite [11], and therefore, there is a maximum for the size of metal nanoparticles. Within the maximum, the size of metal nanoparticles can be tuned by varying the amount of metal salt added to the micellar solution. In theory, it is believed that the micelles are uniformly distributed in the solution. Therefore, the loading of metal salt (L) is defined as:

$$L = N_s / N_v \tag{2}$$

where N_s, N_v represents the total of metal salt molecule and pyridine monomers in solution respectively. Theoretically, L ranges from 0 to 1, so the size of metal nanoparticles can be tuned within the maximum by varying L.

To study the effect of metal salt loading on the size of metal nanoparticles, micelle arrays with different $HAuCl_4$ loading (L=0.1, 0.5, 0.8) were firstly prepared. It is found that the $HAuCl_4$ loading has no influence on the resulting micelle arrays. In other words, the morphology of the micelle arrays remains unchanged under different L. Fig. 4a is the typical AFM image of micelle arrays with different $HAuCl_4$ loading using copolymer PS(1760)-P2VP(700), from which we can see that the micelle particles are well-ordered with a uniform diameter of 70 nm. Then, micelle nanoparticle arrays with different loading (L=0.1, 0.5, 0.8) were exposed to H plasma for 30 min to remove the organic matrix completely, and the resulting Au nanoparticle arrays were shown in Figs. 4b-4d. It can be seen that the quasi hexagonal order and interparticle spacing do not vary with the metal salt loading, while the size of Au nanoparticles increases with L. Under the different value of L: 0.1, 0.5, 0.8, the diameters of the Au nanoparticles are 18, 35 and 45 nm respectively.

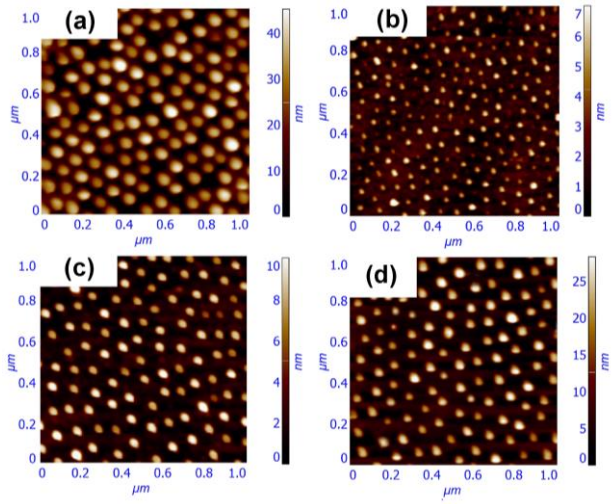

Fig. 4. (black/white) AFM topography images of (a) the micelle array using the copolymer PS(1760)-P2VP(700), and (b)~(d) the resulting Au nanoparticle arrays with the $HAuCl_4$ loading of 0.1, 0.5, 0.8, respectively.

The interparticle spacing of the Au nanoparticle array can also be tuned by varying the drawing velocity in the case of the dip-coating process. It was reported that the CTC distance of the resulting Au nanoparticles decreased with raising the drawing velocity during dip-coating process [2, 3]. On the one hand, the faster the lifting speed, the more solution carried over by the substrate, so there will be more micelle particles involved in self-assembly. On the other hand, different from rigid colloid, the micelle particle is elastic, and the interparticle spacing decreases when micelles squeeze each other, which is in high agree with our results in the following. Figs. 5a-5e show the topography images of Au nanoparticle arrays prepared with the drawing velocities of 3, 6, 10, 15, and 20 mm/min respectively. It can be seeen that the size of the resulting Au nanoparticles does not vary with the drawing velocity, whereas the interparticle spacing decreases gradually as the drawing velocity increases. The average CTC distances of the neighboring Au nanoparticles, derived from the AFM images shown in Figs. 5a-5e, are plotted in Fig. 5f as a function of the drawing velocity *U*. In agreement with the spectral evolution, a linear fitted dashed line was obtained, indicating that the interparticle spacing are inversely proportional to $U^{1/3}$, which is in accordance with the model for dip-coating processes proposed in other reports [2, 12].

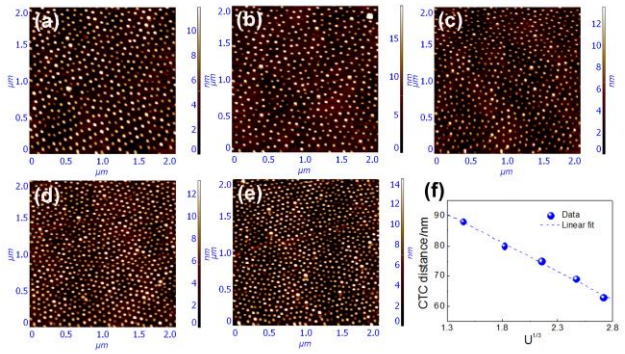

Fig. 5. (black/white) AFM topography images of Au nanoparticle arrays prepared with various drawing velocities: (a) 3, (b) 6, (c) 10, (d) 15, (e) 20 mm/min using diblock-copolymer PS[1779]-b-P2VP[357]. (f) plot of the average CTC distances of Au nanoparticle arrays as a function of the drawing velocity U.

As mentioned above, metal nanoparticle arrays, such as Au, Ag or Pt, can be used as LSP to enhance the performance of LEDs and solar cells. Besides, we can probably tune the properties of LSP by varying the particle size or interparticle spacing. The effect of particle size on the LSP resonance position and strength has been reported repeatedly [13-15], so we studied the characteristics of LSP by varying the interparticle spacing of Au nanoparticle arrays. To determine the LSP resonance position of the Au nanoparticle arrays, the extinction spectra of the Au nanoparticle arrays on ITO substrates with different interparticle spacing but same diameter (30 nm) were measured, and the corresponding results are shown in Fig. 6. It can be seen that all the extinction spectra of the Au nanoparticle arrays exhibit an obvious extinction peak at about 550 nm, which remains almost unchanged with increasing the CTC distance from 30 nm to 80 nm. So it is included that the resonance position of LSP resonance does not vary with the interparticle spacing of the metal nanoparticle arrays.

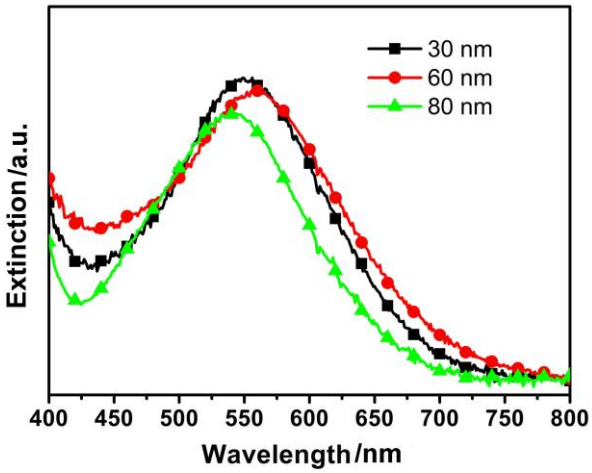

Fig. 6. (black/white) Extinction spectra of Au nanoparticle arrays on ITO substrates with CTC distances of 30, 60, and 80 nm (the mean diameter of the Au nanoparticles is 30 nm).

4. Conclusion

In conclusion, we have prepared Au nanoparticle arrays by a micellar route, and the size and interparticle spacing of the Au nanoparticle arrays are tuned effectively by varying the chain length of the amphiphilic diblock copolymer, the amount of metal salt loading, and the drawing velocity during dip-coating process. Furthermore, as an application example of Au nanoparticle arrays, the characteristics of LSP were studied in detail. Above all, this work provides a route for realizing the promising application of metal nanoparticles in various fields.

Acknowledgements

This work was financially supported by "the Fundamental Research Funds for the Central Universities" (Grant No. 2652013067, 2652012070 and 2652012054), "the National Natural Science Foundation of China" (Grand No. 61106065), and The National Undergraduate Innovative Test Program (Grand No. 201311415038).

References

[1] T. Lohmueller, E. Bock, J. P. Spatz: Adv. Mater. **20**, 2297 (2008).
[2] J. Bansmann, S. Kielbassa, H. Hoster, F. Weig, H. G. Boyen, U. Wiedwald, P. Ziemann, R. J. Behm: Langmuir **23**, 10150 (2007).
[3] S. Qu, X. W. Zhang, Y. Gao, J. B. You, Y. M. Fan, Z. G. Yin, N. F. Chen: Nanotechnology **19**, 135704 (2008).
[4] Y. Gao, X. W. Zhang, Z. G. Yin, S. Qu, J. B. You, N. F. Chen: Nanoscale Res. Lett. **5**, 1 (2010).
[5] D. Takagi, Y. Homma, H. Hibino, S. Suzuki, Y. Kobayashi: Nano Lett. **6**, 2642 (2006).
[6] J. Lu, S. S. Yi, T. Kopley, C. Qian, J. Liu, E. Gulari: J. Phys. Chem. B **110**, 6655 (2006).
[7] J. B. You, X. W. Zhang, J. J. Dong, X. M. Song, Z. G. Yin, N. F. Chen, H. Yan: Nanoscale Res. Lett. **4**, 1121 (2009).
[8] S. G. Zhang, X. W. Zhang, Z. G. Yin, J. X. Wang, J. J. Dong, H. L. Gao, F. T. Si, S. S. Sun, Y. Tao: Appl. Phys. Lett. **99**, 181116 (2011).
[9] H. L. Gao, X. W. Zhang, Z. G. Yin, H. R. Tan, S. G. Zhang, J. H. Meng, X. Liu: Appl. Phys. Lett. **101**, 133903 (2012).
[10] J. P. Spatz, S. Mössmer, C. Hartmann, M. Möller, T. Herzog, M. Krieger, H. G. Boyen, P. Ziemann, B. Kabius: Langmuir **16**, 407 (2000).
[11] S. Förster, M. Zisenis, E. Wenz, M. Antonietti: J. Chem. Phys. **104**, 9956 (1996).
[12] A. A. Darhuber, S. M. Troian, J. M. Davis, S. M. Miller, S. Wagner: J. Appl. Phys. **88**, 5119 (2000).
[13] J. R. Lakowicz: Anal. Biochem. **337**, 171 (2000).
[14] D. Y. Zhang, H. Ushita, P. P. Wang, C. W. Park, R. Murakami, S. C. Yang, X. P. Song: Appl. Phys. Lett. **103**, 093114 (2013).
[15] C. Y. Cho, Y. J. Zhang, E. Cicek, B. Rahnema, Y. B. Bai, R. McClintock, M. Razeghi: Appl. Phys. Lett. **102**, 211110 (2013).

*Corresponding author: jjdong@cugb.edu.cn